

STRAIN-TUNABLE ELECTRONIC PROPERTIES OF CrS₂ NANOTUBES

Y. Z. WANG^{a*}, R. HUANG^a, X. Q. WANG^b, Q. F. ZHANG^c, B. L. GAO^a,
L. ZHOU^a, G. HU^a

^aDepartment of Applied Physics, Huaiyin Institute of Technology, Jiangsu, 223003, China

^bDepartment of Physics, Jinling Institute of Technology, Nanjing, Jiangsu, 211169, China

^cKey Laboratory for Advanced Technology in Environmental Protection of Jiangsu Province, Yancheng Institute of technology, Jiangsu, 224051, China

The electronic and mechanical properties of CrS₂ nanotubes (NTs) are investigated by the first-principles calculations. It is found that both the diameter and chirality of NTs influence on their Young's modulus and Poisson's ratios. The energy band gap and the electron effective mass of NTs would be modulated under the external strain. Although the energy gaps of NTs are not so sensitive to the radial deformation, they change monotonically with the uniaxial strain and insulator-metal transition occurs when the tensile strain increases gradually. Our results highlight the strain-tunable electronic properties of CrS₂ nanotubes, which is a promising candidate for the applications on nanoscale strain sensor.

(Received May 11, 2016; Accepted July 5, 2016)

Keywords: CrS₂ nanotube, strain, band structure, first-principles calculation

1. Introduction

Since the discovery of carbon NTs in 1991 by Iijima[1], one dimensional NTs have attracted great attention because of their exceptional physical and chemical properties, such as C NTs[2,3], BN NTs[4,5], ZnO NTs[6], GaN NTs[7], MoS₂ NTs[8,9], WS₂ NTs[10,11], SnS₂ NTs[12,13], and so on. Among them, transition metal dichalcogenides (TMDs) such as MoS₂ and WS₂ NTs have attracted huge interest due to their exceptional electronic and optical properties, which make them have many potential applications, such as, lubricants[14], photo-emitting devices[15,16], transistors[17,18], catalysis[19], Li-ion batteries[20]. In recent years, various investigations have been carried out to examine different properties of the MoS₂ and WS₂ NTs. For example, different methods have been developed to fabricate the MoS₂ and WS₂ NTs[20-23]. The structural, mechanical and electronic properties of MoS₂ and WS₂ NTs have been investigated by theory and experiment. Li *et al.* found various defects such as substitution and vacancy can tailor the electronic and magnetic properties of MoS₂ NTs[24]. Li *et al.* have studied the strain-tunable electronic and transport properties of MoS₂ nanotubes[25]. Lu *et al.* investigate the strain-dependent electronic and magnetic properties of MoS₂ monolayer, nanoribbons and nanotubes[26]. In our previous paper, we have studied the structural and electronic of MoS₂ under transverse electric field[27].

As chromium belongs to the same group as molybdenum and tungsten, therefore, monolayer CrS₂ has also attracted great attention because of their electronic and optical properties. Zhang *et al.* have reported the monolayer 2H CrS₂ exhibits a competitive low formation energy and is mechanically, dynamically, and thermally stable; and they find the monolayer CrS₂ has the optical band gap of 1.3 eV[28]. Ataca *et al.* also predict the monolayer is semiconductor with a

*Corresponding author: wuzong@hyit.edu.cn

band gap of 1.07 eV[29]. CrS₂ nanotube can be fabricated by wrapping a CrS₂ monolayer along a chiral vector. To the best of our known, the structure, mechanical and electronic of the CrS₂ NTs is still lack.

In this paper, we systematically investigate the structural, mechanical and strain tunable electronic properties of the CrS₂ NTs. We observe the Young's modulus and Poisson ratio of the NTs are dependent on the diameter and chirality. The band gap and effective mass of electron of the CrS₂ NTs can be tuned by the uniaxial strain, but it is dependent on the chirality. Furthermore, the radial compressive strain can reduce slightly the band gap, meanwhile, it can slightly increase the effective mass of electron of the CrS₂ NTs.

2. Computational methods

For the present study, all the calculations are performed within the density functional theory (DFT) using projector-augmented-wave potentials implemented in Vienna ab initio simulation package (VASP)[30-32]. The exchange-correlation potential is described by the generalized gradient approximation (GGA) of the Perdew-Burke-Ernzerhof (PBE) parameterization[33]. A cutoff energy of 500 eV is used for the plane-wave expansion. A k-point mesh of $1 \times 1 \times 11$ is used for sampling the Brillouin zone of the CrS₂ nanotube for the structural optimizations, and thirty k points are sampled for computing the band structure. All the structures are fully optimized with the convergence thresholds of 10^{-5} eV for energy and 0.01 eV/Å for Hellmann-Feynman force. All the CrS₂ NTs are treated within supercell under the periodic boundary conditions. As shown in Fig. 1, the uniaxial compressive and tensile strains are applied along the tube axis by fixing the axial vectors (z) to construct the strained structure. The radial compressive strain is created by a displacement of two outer S atoms along x axis (perpendicular to the tube axis) and fixing them, while other atoms are fully relaxed. To eliminate the interaction between CrS₂ NTs in adjacent supercells, the vacuum spaces are more than 15 Å along the x and y directions.

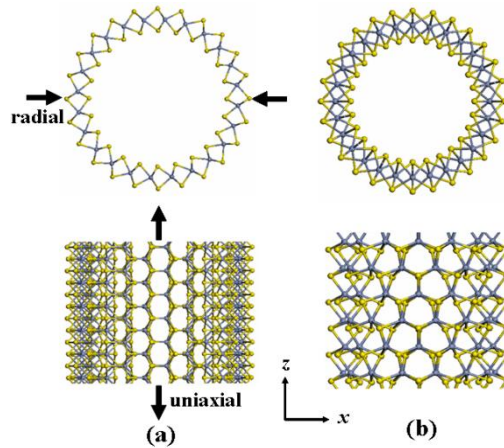


Fig.1. Top and side view of structures of (a) (12, 12) and (b) (14, 0) CrS₂ NTs. The arrow indicates the direction of the strain. The gray atom stands for Cr, and the yellow atom is S.

3. Results and discussion

In order to validate the applied method, at first, we calculate the lattice constant of the unit cell of CrS₂ monolayer. The lattice constant is 3.042 Å, which is consistent with the reported theoretical results[34]. In table1, the optimized values of the lattice constant and radius of the CrS₂ NTs are shown. We find the lattice constant of the zigzag NTs increases with the increasing of the radius, and it will gradually approach the value of 5.269 Å for the monolayer CrS₂. However, for

the armchair NTs, the lattice constant reduces with the increasing of radius, and it will gradually close to the value of 3.042 Å for the monolayer CrS₂.

To character the mechanical properties of the CrS₂ NTs, the Young's modulus Y and Poisson ratio ν are calculated. The Young's modulus indicates the resistance of the NTs to the deformation under uniaxial strain, which can be calculated from the second derivative of the total energy E with respect to the strain ε_{\square} at the equilibrium volume V_0 [25]:

$$Y = \frac{1}{V_0} \times \frac{\partial^2 E}{\partial \varepsilon_{\square}^2} = \frac{1}{2\pi R_0 L_0 \delta} \times \frac{\partial^2 E}{\partial \varepsilon_{\square}^2}$$

where R_0 and L_0 are the radius and the unit cell length of the unstrained NTs, δ indicates the thickness of the tube wall (which is assumed to be 6.147 Å in our calculation). In order to obtain the Young's modulus, the strain energies corresponding to the uniaxial strain between -1% to 1% are calculated. In table 1, it is clearly that the Young's modulus of both armchair and zigzag CrS₂ NTs increase with the increasing of the tube radius. Moreover, for the CrS₂ NTs with the same radius, the Young's modulus of the armchair NTs is larger than that of the zigzag NTs. In earlier study, the Young's modulus of the (10, 0) MoS₂ NT is 127 GPa [25], which is larger than the value of the (10, 0) CrS₂ NT.

Table 1. Calculated lattice constant (L_0) along the z direction, tube radius (R_0), Poisson ratio (ν) and Young's modulus (Y) of CrS₂ NTs.

CrS ₂ nanotube	L_0 (Å)	R_0 (Å)	ν	Y (GPa)
(10, 0)	5.086	5.562	0.318	103.4
(12, 0)	5.138	6.448	0.349	122.2
(14, 0)	5.178	7.336	0.351	132.7
(8, 8)	3.067	7.124	0.350	148.5
(10, 10)	3.058	8.724	0.319	161.4
(12, 12)	3.055	10.328	0.295	168.4

Applying the uniaxial tensile and compressive strain to the CrS₂ NTs can lead the radius to contract and expand. As shown in Fig. 2, for all the CrS₂ NTs, accompanied with the axial elongation, the tube radius reduces gradually. The ratio of transverse contraction and axial elongation is described by Poisson ratio

$$\nu = \frac{\varepsilon_{\perp}}{\varepsilon_{\square}} = -\frac{L_0}{R_0} \times \frac{\partial R}{\partial L}$$

where ε_{\square} is the externally imposed strain along the tube axial direction, and ε_{\perp} is the radial contraction strain. As shown in table 1, the Poisson ratios of the zigzag NTs increase with the increasing of the radius. In contrast, the Poisson ratios of the armchair NTs reduce with increasing radius. The different variation trend of the Poisson ratio for the zigzag and armchair CrS₂ NTs can be attributed to the different orientation of the Cr-S bonds as shown in Fig. 1.

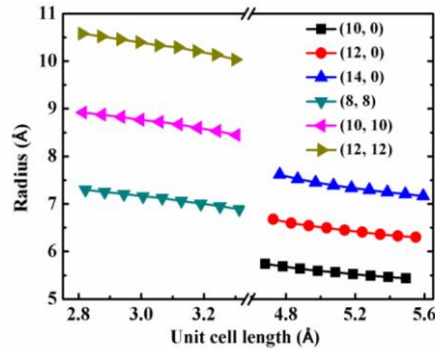


Fig. 2. Nanotube radius with respect to axial unit cell length.

Fig. 3 illustrates the band structures of the zigzag and armchair CrS_2 NTs with and without the external uniaxial strain. We find the (14, 0) zigzag NT exhibits a direct band gap ($E_g = 0.291$ eV) with the valence band maximum (VBM) and conduction band minimum (CBM) at Γ -point. The (12, 12) armchair NT is an indirect band gap ($E_g = 0.575$ eV) with the VBM and CBM at two mid points along Γ -X symmetric lines. From Fig. 3, we also can see compressive (tensile) strain can increase (reduce) the band gap for both zigzag and armchair CrS_2 NTs. The band gap of (14, 0) and (12, 12) CrS_2 NTs can change from 0.382 eV and 0.838 eV at $\varepsilon = -8\%$ to 0.06 eV and 0.276 eV at $\varepsilon = -8\%$. For the (14, 0) zigzag NT, the VBM and CBM always locate at Γ -point under different strain. While, for the (12, 12) armchair NT, the VBM and CBM approach each other along Γ -X line with the strain change from 8% to -8%.

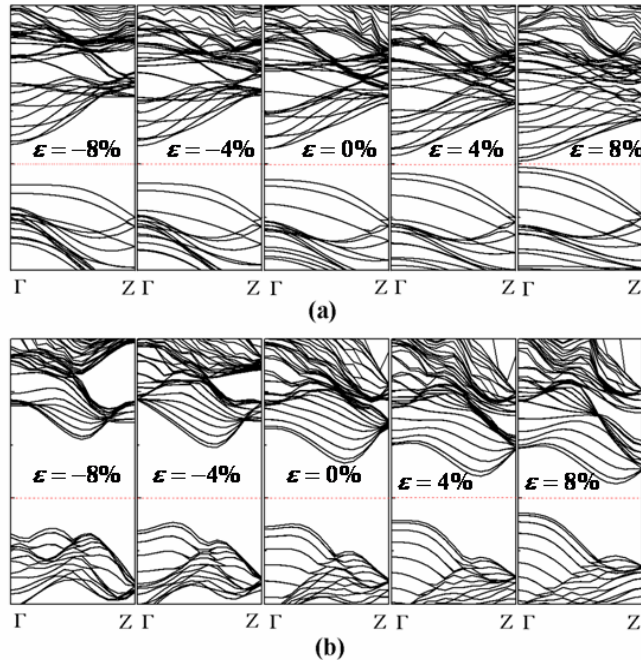


Fig. 3. Band structures of (a) (14, 0) and (b) (12, 12) nanotube under uniaxial strain, respectively.

Fig. 4 shows variations of the band gap of CrS_2 NTs under the uniaxial strain. For the (10, 0) NT with the relatively small radius, the band gap is zero without strain. While, for other NTs, the band gaps increase with the increasing of tube radius without strain. For armchair NTs, the uniaxial

tensile (compressive) strain can linearly decrease (increase) the band gap. The band gap of (14, 0) also linearly reduce under the tensile strain, while the band gap increase in nonlinear fashion under uniaxial compressive strain. Under the compressive strain, the (10, 0) NT can possess no zero band gap. For (12, 0) NT, the band gap reduce to zero at $\varepsilon = 6\%$. Additionally, the slopes of band gap versus strain for the NTs with larger band gap without strain are larger than that of the NTs with smaller band gap. Fig. 5 shows the variation of the band gap of CrS_2 NTs under different radial compressive strain. We find the band gap of the NTs decrease slightly with increasing radial compressive strain except for the (10, 0) NT. Obviously, the axial strain is the more effective method for tuning the band gap than radial strain.

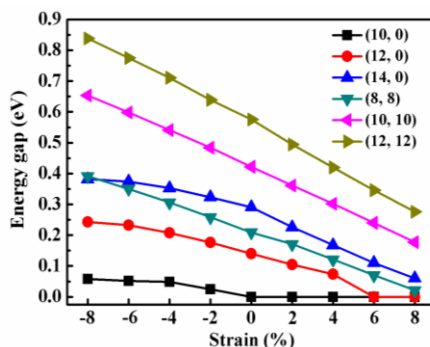


Fig. 4. Energy gap of CrS_2 nanotubes as a function of uniaxial strain.

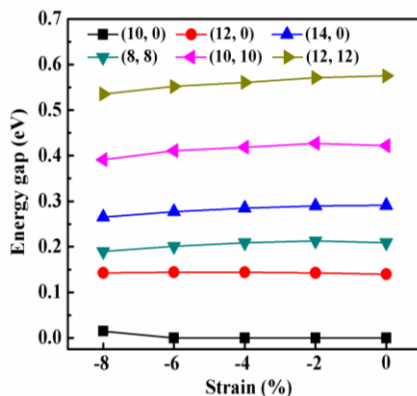


Fig. 5. Energy gap of CrS_2 nanotube as a function of radial strain.

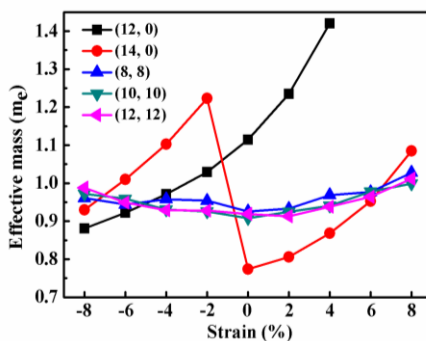


Fig. 6. The effective mass (in units of the free electron mass m_e) of electron for CrS_2 nanotube under uniaxial strain.

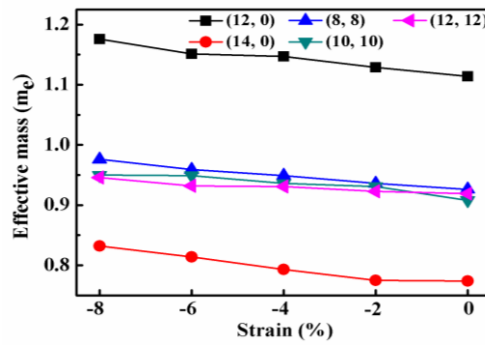


Fig. 7. The effective mass (in units of the free electron mass m_e) of electron for CrS_2 nanotube under radial strain.

From Fig. 3, we can observe strain can also change the energy band curvature besides the band gap, which can lead to changes in the effective mass of electron. It can be calculated using $m^* = \hbar^2 \left[d^2 E(k)/dk^2 \right]^{-1}$, where $E(k)$ is the energy band, k is the coordinate vector in the reciprocal space, and \hbar is the reduced Planck constant. Fig. 6 shows the effective mass of electron under uniaxial strain. Under zero strain, for (8, 8), (10, 10), (12, 12), (12, 0) and (14, 0) NTs, the effective masses of electron are 0.93, 0.91, 0.92, 1.11, and $0.77 m_e$, respectively. These masses are larger than that of monolayer CrS_2 with $m^* = 0.65 m_e$ [28]. For zigzag NTs, it is obvious that the effective mass of electron is sensitive to strain. In contrast, for armchair NTs, both compressive and tensile strains increase slightly the effective mass of electron. Fig. 7 shows the effective mass of electron under radial compressive strain. It can be seen that the effective mass of electron increases gradually with increasing radial compressive strain for all NTs.

4. Conclusions

In summary, the mechanical properties and the effects of different strain on the band structure and effective mass of electron have been studied by first-principle calculations. It is found that the Young's modulus increases with the increasing of the tube diameter for both zigzag and armchair NTs, and the Young's modulus of the armchair NTs is larger than that of the zigzag NTs for the same tube diameter. While the Poisson ratio of the NTs increase (decrease) with the increasing of the radius for zigzag (armchair) NTs. Under uniaxial strain, the band gap of the armchair NTs can vary linearly, while, for the zigzag NTs, the tensile or compressive strain can reduce linearly or increase nonlinearly the band gap, respectively. In addition, the radial compressive strain can also increase slightly the band gap for both the zigzag and armchair NTs. Furthermore, the band gap of the CrS_2 NTs can reduce to zero under the suitable uniaxial tensile strain. In addition, the uniaxial and radial strain can also tune the electron effective mass of the CrS_2 NTs. Our results highlight the strain-tunable electronic properties of CrS_2 NTs, which is a promising candidate for the applications on nanoscale strain sensor.

Acknowledgements

This work was supported by the NSFC (11474246), Foundation of the Jiangsu Higher Education Institutions of China (Grant No. 13KJ430007), and the Qing Lan Project.

References

- [1] S. Iijima, *Nature* **354**, 56 (1991).
- [2] M.M. Shulaker, G. Hills, N. Patil, H. Wei, H.Y. Chen, H.S. PhilipWong, S. Mitra, *Nature* **501**, 526 (2013).
- [3] F. Zhang, P.X. Hou, C. Liu, H.M. Cheng, *Carbon* **102**, 181 (2016).
- [4] A. Vongachariya, V. Parasuk, *Solid State Commun.* **223**, 28 (2015).
- [5] A. Freitas, S. Azevedo, J.R. Kaschny, *J. Solid State Chem.* **233**, 352 (2016).
- [6] Y.Z. Wang, B.L. Wang, Q.F. Zhang, J.J. Zhao, D.N. Shi, S. Yunoki, F.J. Kong, N. Xu, *J. Appl. Phys.* **111**, 073704 (2012).
- [7] D.C. Camacho-Mojica, F. López-Urías, *Sci. Rep.* **5**, 17902 (2015).
- [8] D.B. Zhang, T. Dumitrica, G. Seifert, *Phys. Rev. Lett.* **104**, 065502 (2010).
- [9] R.F. Cao, B. Zhou, C.F. Jia, X.D. Zhang, Z.Y. Jiang, *J. Phys. D: Appl. Phys.* **49**, 045106 (2016).
- [10] K.R. O'Neal, J.G. Cherian, A. Zak, R. Tenne, Z. Liu, J.L. Musfeldt, *Nano Lett.* **16**, 993 (2015).
- [11] R. Levi, J. Garel, D. Teich, G. Seifert, R. Tenne, E. Joselevich, *ACS Nano* **9**, 12224 (2015).
- [12] Y.C. Huang, C.Y. Ling, X. Chen, D.M. Zhou, S.F. Wang, *RSC Adv.* **5**, 32505 (2015).
- [13] A.V. Bandura, R.A. Evarestov, *Surf. Sci.* **641**, 6 (2015).
- [14] J. Jelenc, M. Remskar, *Nanoscale Res. Lett.* **7**, 208 (2012).
- [15] J.P. Mathew, G. Jegannathan, S. Grover, P.D. Dongare, R.D. Bapat, B.A. Chalke, S.C. Purandare, M.M. Deshmukh, *Appl. Phys. Lett.* **105**, 223502 (2014).
- [16] B. Visic, R. Dominko, M.K. Gunde, N. Hauptman, S.D. Skapin, M. Remskar, *Nanoscale Res. Lett.* **6**, 593 (2011).
- [17] M. Strojnik, A. Kovic, A. Mrzel, J. Buh, J. Strle, D. Mihailovic, *AIP Adv.* **4**, 097114 (2014).
- [18] S. Fathipour, M. Remskar, A. Varlec, A. Ajoy, R. Yan, S. Vishwanath, S. Rouvimov, W.S. Hwang, H.G. Xing, D. Jena, A. Seabaugh, *Appl. Phys. Lett.* **106**, 022114 (2015).
- [19] K. Xu, F.M. Wang, Z.X. Wang, X.Y. Zhan, Q.S. Wang, Z.Z. Cheng, M. Safdar, J. He, *ACS Nano* **8**, 8468 (2014).
- [20] G.D. Li, X.Y. Zeng, T.D. Zhang, W.Y. Ma, W.P. Li, M. Wang, *CrystEngComm* **16**, 10754 (2014).
- [21] M. Remskar, A. Mrzel, Z. Skraba, A. Jesih, M. Ceh, J. Demšar, P. Stadelmann, F. Lévy, D. Mihailovic, *Science* **292**, 479 (2001).
- [22] M. Nath, A. Govindaraj, C.N.R. Rao, *Adv. Mater.* **13**, 283 (2001).
- [23] O. Brontvein, V. Jayaram, K.P.J. Reddy, J.M. Gordon, R. Tenne, *Z. Anorg. Allg. Chem.* **640**, 1152 (2014).
- [24] N. Li, G. Lee, Y.H. Jeong, K.S. Kim, *J. Phys. Chem. C* **119**, 6405 (2015).
- [25] W. Li, G. Zhang, M. Guo, Y.W. Zhang, *Nano Research* **7**, 518 (2014).
- [26] P. Lu, X.J. Wu, W.L. Guo, X.C. Zeng, *Phys. Chem. Chem. Phys.* **14**, 13035 (2012).
- [27] Y.Z. Wang, B.L. Wang, Q.F. Zhang, R. Huang, B.L. Gao, F.J. Kong, X.Q. Wang, *Chalcogenide Lett.* **11**, 493 (2014).
- [28] H.L. Zhuang, M.D. Johannes, M.N. Blonsky, R.G. Hennig, *Appl. Phys. Lett.* **104**, 022116 (2014).
- [29] C. Ataca, H. Şahin, S. Ciraci, *J. Phys. Chem. C* **116**, 8983 (2012).
- [30] P.E. Blöchl, *Phys. Rev. B* **50**, 17953 (1994).
- [31] G. Kresse, J. Furthmüller, *Comp. Mater. Sci.* **6**, 15 (1996).
- [32] G. Kresse, J. Furthmüller, *Phys. Rev. B* **54**, 11169 (1996).
- [33] J.P. Perdew, K. Burke, M. Ernzerhof, *Phys. Rev. Lett.* **77**, 3865 (1996).
- [34] H.Y. Guo, N. Lu, L. Wang, X.J. Wu, X.C. Zeng, *J. Phys. Chem. C* **118**, 7242 (2014).